A Benchmark for 3D Reconstruction from Aerial Imagery in an Urban Environment

Susana Ruano[1], Aljosa Smolic[1]
[1]*V-SENSE, Trinity College Dublin, Ireland*
ruanosas, smolica@scss.tcd.ie

Keywords: Benchmark, 3D Reconstruction, Structure-from-Motion, Multi-View Stereo

Abstract: This paper presents a novel benchmark to evaluate 3D reconstruction methods using aerial images in a large-scale urban scenario. In particular, it presents an evaluation of open-source state-of-the-art pipelines for image-based 3D reconstruction including, for the first time, an analysis per urban object category. Therefore, the standard evaluation presented in generalist image-based reconstruction benchmarks is extended and adapted to the city. Furthermore, our benchmark uses the densest annotated LiDAR point cloud available at city scale as ground truth and the imagery captured alongside. Additionally, an online evaluation server will be made available to the community.

1 INTRODUCTION

Creating 3D models from a collection of images is a classic problem in computer vision (Hartley and Zisserman, 2003), it has been extensively studied (Snavely et al., 2008; Sweeney et al., 2015; Moulon et al., 2013; Schönberger and Frahm, 2016; Furukawa and Ponce, 2010; Barnes et al., 2009; Schönberger et al., 2016) and it is used in fields such as augmented and virtual reality (Ruano et al., 2017; Pagés et al., 2018). The common procedure to generate a 3D reconstruction from a collection of images begins with the detection and matching of features which are given as input to a Structure-from-Motion (SfM) algorithm to recover the camera poses and a sparse model (Snavely et al., 2008). Then, to densify the skeleton of the reconstruction given by the sparse 3D point cloud a Multi-View Stereo (MVS) algorithm is applied (Hartley and Zisserman, 2003). The methods can be configured according to the particularities of the scene (e.g., smoothness of the terrain (Ruano et al., 2014)) but the majority of them considers general scenarios and specially, the ones which are open-source are widely used (Stathopoulou et al., 2019).

Despite the constant and recent progress in 3D reconstruction techniques, one of the problems that has been pointed out is the lack of ground-truth models to test the algorithms (Schops et al., 2017; Knapitsch et al., 2017). These models are difficult to obtain with the appropriate density and quality because their collection is usually done with active techniques that require special equipment (e.g., LiDAR) and it is not always accessible. Still, some efforts were made in the past to fulfill those necessities and several benchmarks were created (Seitz et al., 2006; Schops et al., 2017; Knapitsch et al., 2017). This ranges from the first widely known Middlebury benchmark (Seitz et al., 2006) with only two pieces of ground truth captured indoors in a controlled environment, to the latest releases such as ETH3D (Schops et al., 2017) and Tanks and Temples (Knapitsch et al., 2017), which include outdoor areas.

A commonality in recent benchmarks is that the challenges for the reconstruction methods are based on the variety of scenarios they provide to do the evaluation. Although this is a valid strategy, urban scenarios can provide itself with a great variety of challenges, even in the same city, due to the heterogeneity of elements that can be found there. As suggested in (Zolanvari et al., 2019), the analysis of a reconstruction in terms of categories of elements of a city will be of interest to support the observations that can be done about different parts of the city with quantitative measurements. Fortunately, the interest of the community in deep learning techniques with 3D data has pushed the creation of ground-truth data with a categorization of urban elements but, still there are new benchmarks focusing on urban environments which do not incorporate this information in their 3D reconstruction analysis (Özdemir et al., 2019).

In this paper, we present a benchmark that offers an extensive evaluation for 3D reconstruction algo-

rithms thanks to a broad study of a large urban environment. It uses as ground truth the densest annotated point cloud available at city scale, DublinCity (Zolanvari et al., 2019), which presents a remarkable level of detail in the annotations allowing for an evaluation of image-based 3D reconstruction methods not only at scene level but also per category of urban element, which is a unique feature compared to previous available benchmarks. The benchmark includes three different sets of images that are created from aerial images with two different camera configurations. Furthermore, we provide online evaluation so new 3D reconstruction methods can be assessed through a common comparative evaluation setup.

2 RELATED WORK

The first widely known benchmark for MVS is the Middlebury (Seitz et al., 2006), which consists of two ground-truth models captured with a laser stripe scanner and three different sets of images per model. This benchmark was later extended in (Aanæs et al., 2016), where they increased the number of considered 3D models with corresponding images, with different lighting conditions for each set. However, both of them were captured in a controlled environment and lack of any scene outside of the laboratory. One benchmark that overcomes the limitation of providing ground truth only in a confined space is the EPFL benchmark (Strecha et al., 2008), which includes realistic scenes captured outdoors with a terrestrial LiDAR. This was an advantage compared to previous ones but they only covered a few scenarios such as a facade of a building or a fountain. Further, it has the limitation of terrestrial LiDAR which can only partially cover the scenes.

The ETH3D benchmark (Schops et al., 2017) however, shows a wide variety of indoor and outdoor scenarios. In particular, different areas are covered (e.g., a courtyard, a meadow, a playground) to test the algorithms against different challenges. However, the models were captured with a terrestial LiDAR and they do not provide details of the tops of the buildings such as the roofs. At a similar time the Tanks and Temples (Knapitsch et al., 2017) benchmark was released, which also gained a lot of interest. The main difference to ETH3D, is that they use video as input, and they evaluate the complete pipeline including SfM and MVS, not only MVS, because they want to stimulate research that solves the image-based 3D reconstruction problem as a whole, including the estimation of the camera positions. Other benchmarks which are solely focused on urban

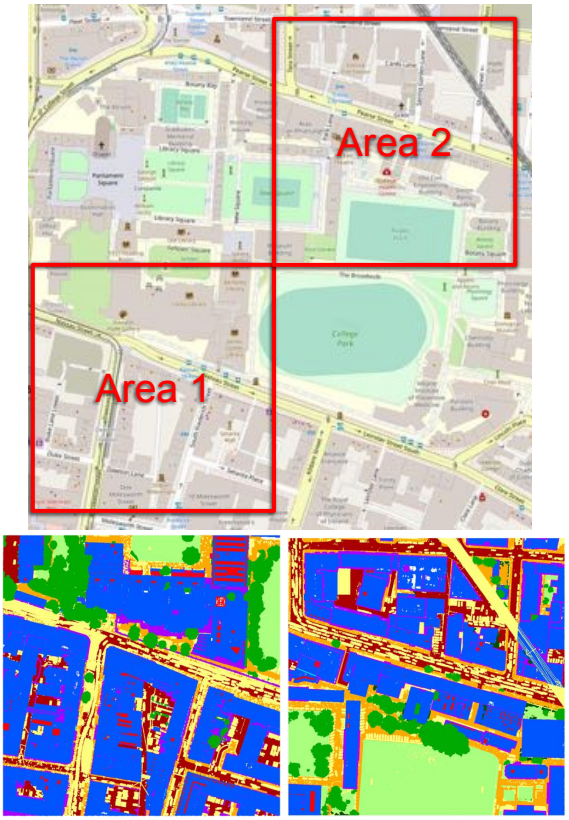

Figure 1: **Areas evaluated in the benchmark.** At the top, the areas of the the city under study are overlaid in the map. At the bottom, a top view of the ground truth of each area is depicted with a different color per class. Area 1 is on the left and Area 2 is on the right.

environments are the Kitti benchmark (Menze and Geiger, 2015) and the TerraMobilita/iQmulus benchmark (Vallet et al., 2015). Both of them use 3D Mobile Laser Scanning (MLS) as ground truth. The former includes the images captured alongside to evaluate several tasks such as scene flow, stereo, object detection but it does not include neither aerial data nor a specific MVS evaluation. The latter only provides annotated 3D data, similar to the Paris-rue-madame dataset (Serna et al., 2014) and the Oakland 3D Point Cloud dataset (Munoz et al., 2009), but no images are included and therefore the evaluation is done for tasks like object segmentation and object classification.

The Toronto/Vaihingen ISPRS benchmark used in (Zhang et al., 2018) is not limited by the use of MLS to create the ground-truth model. However, although a large-scale urban scenario is covered, the 3D building models are not created from the images, they are created from the Aerial Laser Scan (ALS) point cloud. Also, Urban Semantic 3D data (Bosch et al., 2019) is a large-scale public dataset that includes semantic labels for two large cities but it uses satellite

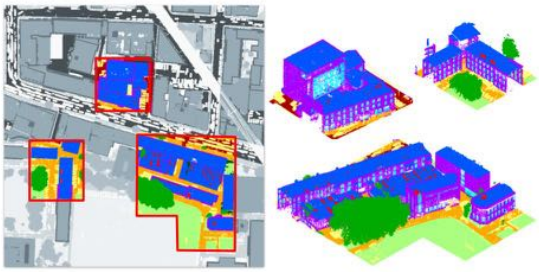

Figure 2: **Hidden areas.** On the left, an example of a hidden area (in color) over the whole region (in grey). On the right, the hidden area represented in 3D.

imagery and they do not provide a semantic evaluation of the 3D reconstruction. The ISPRS Test project on Urban Classification and 3D Building Reconstruction (Rottensteiner et al., 2014) have airborne images but the number of images offered is no more than 20 per area, the benchmark reconstruction task is focused on roofs, the density of the ALS is 6 points per m^2, and they only provide one type of images per set. One of the most recent annotated LiDAR point clouds captured with ALS is DublinCity (Zolanvari et al., 2019), which also includes airborne images associated (Laefer et al., 2015). The average density of the ALS point cloud is remarkable compared to other existing datasets (i.e., 348.43 points/m^2) and the LiDAR point cloud is used as ground truth for the evaluation of an image-based 3D reconstruction, but they do not include the annotations in the evaluation.

3 BENCHMARK DATASET

Area selection. The initial dataset of Dublin city center (Laefer et al., 2015) and the annotations incorporated in (Zolanvari et al., 2019) are used for the creation of this benchmark. We analysed the whole annotated dataset (the potential ground truth) to ensure that the selected areas constitute a good representation of the city and also, that they have a balanced distribution of points in each category, so content diversity and representativeness is guaranteed for an evaluation per urban object category. The criteria used to choose the specific tiles for evaluation are based on the area of the city covered, the variety of the city elements in them and the avoidance of potential sources of errors.

In particular, we have discarded the ones that are covering less than 250×250 m^2 of the city, the ones that include less than 1% of points corresponding to grass and less than 4% of points corresponding to trees. Also, we discarded tiles with points in the undefined class above 10% and the ones containing cranes, because they may degrade performance. With these criteria two tiles are left, that will be the areas used in this benchmark, shown in Fig. 1 and will allow us to have a representative part of the city while keeping the amount of data that have to be processed reasonable.

(a) (b)

Figure 3: **Images.** (a) a sample of the nadir set of images; (b) a sample of the oblique one.

Hidden areas. We are also evaluating a specific region in each area that will not be revealed to the user to avoid fine tuning during online evaluation (see Section 4). We call these regions *hidden areas* and we show an example of a potential hidden area in Fig. 2. As it can be seen, they consist of meaningful sections of the city spread across the ground truth (each of them including several classes). We have selected them taking the class distribution into account but the exact portions of the ground truth that belongs to the hidden area are not revealed.

Area description. We are evaluating two different regions of the city of Dublin (depicted in red in Fig. 1) which were selected following the aforementioned analysis. *Area 1* encompasses the south west part of Trinity College Dublin (TCD) campus, several streets of the city, buildings and green areas. *Area 2* includes the north east of the TCD campus, different buildings, streets and it includes parts of rail tracks.

Table 1 shows the distribution of the classes in terms of number of points and the percentage of points in the whole ground truth and the hidden areas. It can be seen that the most populated class is roof and the one with least representation is doors. Nevertheless, the percentage of the class roof in the hidden areas is more balanced with the other classes. It can also be observed that the undefined data, which is a potential source of inaccuracies, represents between 5% and 9% of the points. *Area 1* has almost double of points in the window category and almost four times of windows in the roof. Furthermore, *Area 2* triples the number of points associated with grass in *Area 1*.

For each area, three different sets of images are used to create the reconstructions: oblique, nadir and combined. Oblique and nadir contain images from the homonyms groups explained in (Zolanvari et al., 2019) and a sample of each group is shown in Fig. 3. The combined group contains the images from both of them. The initial dataset contains a large number of

		undefined	facade	window	door	roof	r. window	r. door	sidewalk	street	grass	tree
Area 1	# points ($\times 10^3$)	1397	3048	540	40	10727	481	3	2029	3210	1587	3471
	percentage	5.27	11.49	2.04	0.15	40.43	1.81	0.01	7.65	12.10	5.98	13.08
	hidden # p. ($\times 10^3$)	1015	1816	312	27	2849	247	2	1602	2441	1353	2720
	hidden pct.	7.06	12.63	2.17	0.19	19.81	1.72	0.01	11.14	16.97	9.41	18.91
Area 2	# points ($\times 10^3$)	1615	2776	308	40	7807	112	3	2789	2642	4061	2852
	percentage	6.46	11.10	1.23	0.16	31.22	0.45	0.01	11.15	10.57	16.24	11.41
	hidden # p. ($\times 10^3$)	1262	1547	220	27	2708	47	1	2010	1993	2226	1897
	hidden pct.	9.05	11.105	1.58	0.19	19.43	0.34	0.01	14.42	14.30	15.97	13.61

Table 1: Number of points and percentage of points per class in each evaluated area. Also the number of points and percentage used as the hidden zone.

oblique and nadir images, many more than needed for a meaningful 3D reconstruction of a particular area. Further, it is not obvious which images are associated with a certain area. In order to identify a meaningful subset of images, we ran the COLMAP SfM algorithm (Schönberger and Frahm, 2016) with all the oblique images of the initial dataset. We then selected the subset of images, where each generated at least 1500 3D points in the areas under evaluation. The same process was done with the nadir images.

4 EVALUATION

Pipelines tested. In this benchmark, we evaluate the 3D dense point cloud obtained when an image-based reconstruction pipeline is applied to a collection of aerial images. Usually, research is focused on solving one specific problem of the pipeline: SfM or MVS. However, we want to allow the possibility of evaluating new techniques that can solve the problem with a different approach, not necessarily applying SfM followed by MVS. Furthermore, as we are not in a controlled environment, we do not have the camera positions with accuracy to be used as ground-truth. Instead, we have the GPS, which is only a coarse approximation. For these reasons, we are only evaluating the final 3D reconstruction, not the intermediate steps.

To do the state-of-the-art evaluation we have selected different pipelines that were studied in the latest comparison of open-source 3D reconstruction methods (Stathopoulou et al., 2019). Following this approach we established the pipelines assembling compatible SfM and MVS methods. In particular, for SfM, we use COLMAP (Schönberger and Frahm, 2016) which includes a geometric verification strategy to improve robustness on initialization and triangulation and an improved bundle adjustment strategy with an outlier filtering strategy. Besides, we selected OpenMVG with two different approaches: global (Moulon et al., 2013), with a global calibration approach based on the fusion of relative motions between image pairs; and incremental (Moulon et al., 2012), that iteratively adds new estimations to an initial reconstruction minimizing the drift with successive steps of non-linear refinement. Furthermore, for MVS, we choose COLMAP (Schönberger et al., 2016) that makes a joint estimation of depth and normal information and makes a pixelwise view selection using photometric and geometric priors. We also use OpenMVS (Schönberger et al., 2016), that uses an efficient patch based stereo matching followed by a depth-map refinement process. In (Stathopoulou et al., 2019), AliceVision was also tested, but we are not including it in our evaluation because it directly produces a mesh, without providing a dense point cloud representation as an exploitable intermediate step. However, AliceVision is based on the incremental OpenMVG (Moulon et al., 2012) and the CMPMVS (Jancosek and Pajdla, 2011) which can handle weakly textured surfaces. We selected the former method for SfM but the latter is no longer publicly available. To sum up, Fig. 4 shows the details of the six pipelines tested in the benchmark: (1) COLMAP(SfM) + COLMAP(MVS); (2) COLMAP(SfM) + OpenMVS; (3) OpenMVG-g + COLMAP(MVS); (4) OpenMVG-g + OpenMVS; (5) OpenMVG-i + COLMAP(MVS); (6) OpenMVG-i + OpenMVS. The version of COLMAP, OpenMVG and OpenMVS used are v3.6, v1.5 and v1.1 respectively, and, as it is depicted in the figure, four stages are needed: SfM, geo-registration, data preparation and MVS. The SfM step includes the feature detection and matching provided by each of the methods used. The parameters used for COLMAP are the same as in DublinCity (Zolanvari et al., 2019), and the param-

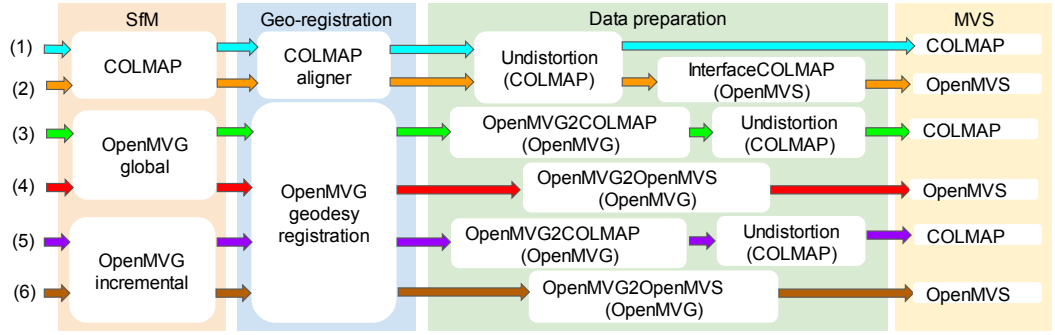

Figure 4: **Scheme of 3D reconstruction pipelines tested.** (1) COLMAP+COLMAP, (2) COLMAP+OpenMVS, (3) OpenMVGg+COLMAP, (4) OpenMVGg+OpenMVS, (5) OpenMVGi+COLMAP, (6) OpenMVGi+OpenMVS.

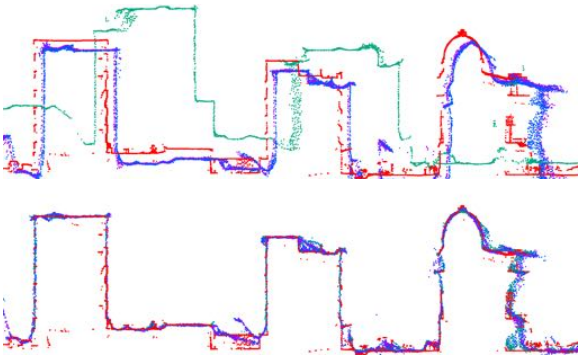

Figure 5: **Registration.** Skyline of the ground-truth (in red) against the 3D reconstructions with oblique (in green), nadir (in purple) and the combined (in blue) sets of images. On the top, the coarse registration, at the bottom, the fine one.

eters used for OpenMVG are the default: SIFT for feature detection, essential matrix filtering for computing matches for global, and fundamental matrix filtering for incremental. After the SfM is done, the geo-information of the dataset is used for a coarse registration of the point cloud (i.e, geo-registration), and we use the methods provided by COLMAP and OpenMVG.

After the geo-registration is done, we have to prepare the data to be densified. For that reason, we use the different procedures proposed for each method for converting the formats and undistorting the images. We used the same parameters each time we applied the same procedure. Finally, the last step is the densification which is done with the recommended parameters in COLMAP and OpenMVS except when an image reduction was needed for OpenMVS. In that case, we used the parameters reported in the ETH3D benchmark which were not hard-coded.

Alignment. The strategies for the alignment of the 3D reconstructions with the ground truth usually consist of two steps: a coarse alignment followed by the refinement of the initial estimation. In our evaluation, the coarse registration is done in the geo-registration step of the pipelines, and as a consequence, the dense point clouds generated are already coarsely registered with the LiDAR scan. As an example, the results of the coarse registration with the COLMAP + COLMAP pipeline are shown on the left in Fig. 5. The skyline of the ground truth is depicted in red and the 3D reconstructions in blue (oblique images), green (nadir images) and purple (combined).

The refinement of the registration is commonly done applying a 7DoF ICP algorithm. This is the strategy followed in (Knapitsch et al., 2017). A more sophisticated approach is used in (Schops et al., 2017), but they use the color information of the laser scan, which is not available in our benchmark. In our approach, we use the point cloud obtained from the first pipeline to refine the coarse registration with the ground-truth applying an ICP algorithm. Then, for the rest of the pipelines, we use the camera positions of the already refined one as a reference, and we apply the same ICP algorithm to obtain the transformations that will align the cameras. After that, we apply the transformation to the entire 3D point clouds. For online evaluation using our benchmark we will require the input 3D point cloud to be already registered, which will allow users to use and optimize their own registration.

Measurements. For the evaluation we use the measurements proposed in (Knapitsch et al., 2017; Zolanvari et al., 2019). In particular, we use: precision, P, recall, R and F score, F. The precision, shows how closely the reconstruction is to the ground truth, the recall, is related to how complete the reconstruction is, and the F score, is a combination of both. Other measurements as the mean distance between the point clouds could be used as in (Stathopoulou et al., 2019), but the advantage of the selected ones is that they are less affected by outliers. They are defined in Eq. (1), Eq. (2), Eq. (3), respectively, for a given threshold distance d. In the equations, I is the point cloud under evaluation and G is the ground-truth

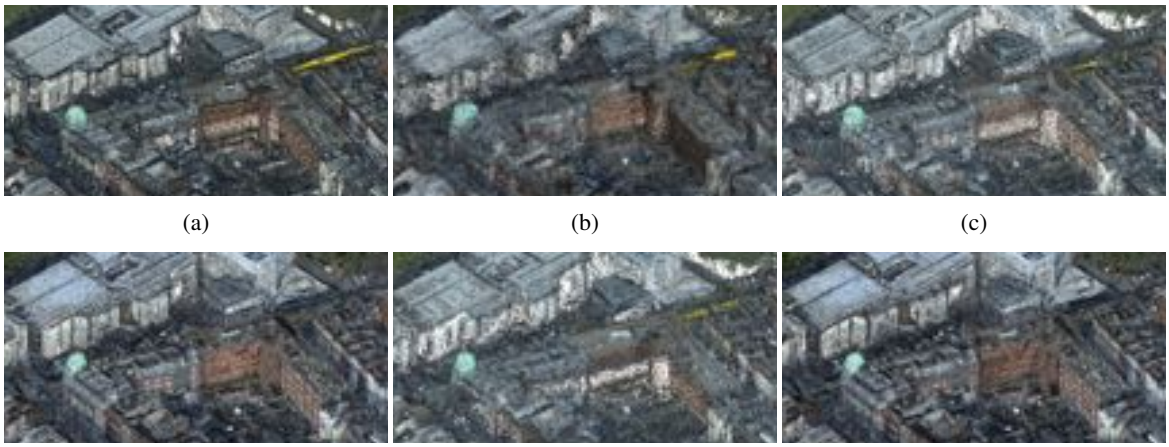

(a) (b) (c)

(d) (e) (f)

Figure 6: **Qualitative 3D reconstruction results.** Point clouds obtained with the oblique and nadir images combined in *Area 1* with each of the pipelines tested (a) COLMAP + COLMAP, (b) COLMAP + OpenMVS, (c) OpenMVG-g + COLMAP, (d) OpenMVG-g + OpenMVS, (e) OpenMVG-i + COLMAP, (f) OpenMVG-i + OpenMVS.

point cloud. $|\cdot|$ is the cardinality and $dist_{I\to G}(d)$ are the points in I with a distance to G less than d and $dist_{G\to I}(d)$ is analogous (i.e., $dist_{A\to B}(d) = \{a \in A \mid \min_{b\in B} \|a-b\|_2 < d\}$, A and B being point clouds).

$$P(d) = \frac{|dist_{I\to G}(d)|}{|I|} 100 \tag{1}$$

$$R(d) = \frac{|dist_{G\to I}(d)|}{|G|} 100 \tag{2}$$

$$F(d) = \frac{2P(d)R(d)}{P(d)+R(d)} \tag{3}$$

To perform the evaluation per class, the point under evaluation will be given the same class as its nearest neighbor in the ground-truth.

Online evaluation. We will provide online evaluation[1] of the 3D reconstructions to stimulate and support progress in the field. The users should provide the final dense point cloud already registered to the ground truth. This will be possible because the ground truth will be publicly available. To ensure a fair comparison, we will be calculating the precision, recall and F score not only in the complete ground truth but also in the hidden areas.

5 RESULTS

We report the precision, recall and F score values for each selected pipeline, set of images and area, including the hidden parts. The measurements were calculated with d in the range of 1 cm to 100 cm obtaining, as expected, an increasing performance in every method when a further distance was considered. We report the results at 25 cm, similar to (Zolanvari et al., 2019), as a good compromise between the limitations of the image resolution and the meaningfulness of the precision, since selecting a very small distance would mean poorer performances for all the methods and with a larger distance the precision would be less informative.

Scene level evaluation. Table 2 shows the evaluation of the pipelines' outcomes against the ground-truth models without considering the urban element category. From these measurements, we can observe that reconstructions from oblique imagery as input, achieve the lowest recall values in all the areas. Therefore, the precision has a main role in achieving a high F score for this image set category. In particular, COLMAP + COLMAP has the best performance (F score) with that type of imagery in every area. Additionally, the reconstructions done with the nadir image set have higher recall values than the ones with the oblique imagery. Also, the recall is usually higher than the precision for these sets so the accuracy is not as determinant as in the oblique sets. As can be observed, COLMAP + COLMAP is the best pipeline in *Area 1* whereas OpenMVG-i + OpenMVS is the best in *Area 2* (even in the hidden parts). These results suggest that having different camera angles and less coverage of the same parts of the scene (as it is the case in the oblique set and not in the nadir one) makes the recall value decrease while the precision remains similar.

For the reconstructions obtained with the com-

[1] https://v-sense.scss.tcd.ie/research/6dof/benchmark-3D-reconstruction

	Area 1			*Area 2*		
	oblique	nadir	oblique and nadir	oblique	nadir	oblique and nadir
(1)	**79.18** / 60.5 / **68.59**	**73.08** / 68.98 / **70.97**	74.89 / 74.15 / 74.52	**80.48** / 65.51 / **72.23**	74.97 / 72.34 / 73.63	76.54 / 77.98 / 77.25
(2)	22.74 / 28.28 / 25.21	23.96 / 46.23 / 31.57	27.93 / 60.84 / 38.29	26.85 / 41.81 / 32.7	24.45 / 49.96 / 32.83	24.7 / 63.53 / 35.57
(3)	49.42 / 13.09 / 20.69	44.02 / 47.95 / 45.9	48.74 / 58.24 / 53.07	36.92 / 15.7 / 22.03	33.26 / 36.4 / 34.76	41.94 / 50.3 / 45.74
(4)	61.07 / 57.1 / 59.02	56.61 / **73.46** / 63.94	**78.27** / **80.49** / **79.36**	40.23 / 54.27 / 46.21	**75.2** / 75.92 / **75.56**	79.3 / 82.03 / 80.64
(5)	37.13 / 16.59 / 22.94	36.59 / 43.62 / 39.8	39.48 / 51.36 / 44.64	38.11 / 15.11 / 21.64	43.76 / 52.0 / 47.52	36.62 / 48.53 / 41.74
(6)	55.12 / **64.37** / 59.39	49.14 / 70.75 / 58.0	74.19 / 79.5 / 76.76	58.52 / **70.43** / 63.92	71.44 / **79.0** / 75.03	**79.77** / **82.54** / **81.13**
	hidden *Area 1*			hidden *Area 2*		
	oblique	nadir	oblique and nadir	oblique	nadir	oblique and nadir
(1)	**78.68** / 49.89 / **61.06**	**72.69** / 62.77 / **67.37**	74.54 / 68.34 / 71.3	**80.06** / 61.48 / **69.55**	73.63 / 68.9 / 71.18	75.5 / 75.27 / 75.39
(2)	23.55 / 18.97 / 21.01	24.42 / 36.88 / 29.39	28.38 / 50.45 / 36.32	27.05 / 37.02 / 31.26	24.24 / 43.98 / 31.25	24.4 / 56.88 / 34.15
(3)	43.12 / 6.61 / 11.46	42.52 / 38.01 / 40.14	48.48 / 48.74 / 48.61	36.47 / 13.19 / 19.37	33.08 / 31.82 / 32.43	40.97 / 43.7 / 42.29
(4)	56.57 / 48.7 / 52.34	56.03 / **69.48** / 62.03	**75.36** / **75.76** / **75.56**	40.31 / 54.08 / 46.19	**74.93** / 74.31 / **74.62**	77.19 / 79.52 / 78.34
(5)	30.83 / 8.88 / 13.79	36.51 / 35.47 / 35.98	38.79 / 42.08 / 40.37	35.24 / 12.3 / 18.24	43.7 / 47.28 / 45.42	35.35 / 42.39 / 38.55
(6)	52.93 / **59.33** / 55.95	48.47 / 67.81 / 56.53	70.56 / 75.02 / 72.72	56.16 / **67.58** / 61.34	67.99 / **77.08** / 72.25	**78.38** / **80.49** / **79.42**

Table 2: **Quantitative results with the whole ground-truth.** Each row shows the results of a specific 3D reconstruction pipeline giving the precision / recall / F score for d=25cm obtained for the reconstruction in each set of images in each area. The best score for each area and image set is in bold letters and the pipelines are as follow: (1) COLMAP + COLMAP, (2) COLMAP + OpenMVS, (3) OpenMVG-g + COLMAP, (4) OpenMVG-g + OpenMVS, (5) OpenMVG-i + COLMAP, (6) OpenMVG-i + OpenMVS.

	F SCORE					
	Area 1 - *Area 1* hidden			*Area 2* - *Area 2* hidden		
	oblique	nadir	combined	oblique	nadir	combined
facade	58.34 (1) - 57.1 (1)	59.96 (4) - 59.08 (4)	67.01 (4) - 65.91 (4)	63.12 (1) - 62.17 (1)	67.7 (6) - 65.82 (6)	**71.73 (6)** - **70.83 (6)**
window	58.83 (1) - 58.18 (1)	53.92 (4) - 53.83 (4)	62.41 (1) - 62.45 (1)	55.06 (1) - 57.2 (1)	61.73 (6) - 60.9 (6)	**63.34 (6)** - **63.59 (6)**
door	41.97 (1) - 45.46 (1)	51.55 (4) - 52.55 (4)	53.14 (4) - 52.96 (4)	49.18 (6) - 48.63 (6)	53.84 (6) - 51.07 (6)	**56.57 (6)** - **56.69 (6)**
roof	80.78 (1) - 75.55 (1)	80.18 (1) - 77.39 (1)	**87.98 (4)** - **85.55 (4)**	81.57 (1) - 80.66 (1)	81.41 (1) - 80.06 (1)	86.05 (6) - 85.53 (6)
r. window	77.33 (1) - 77.67 (1)	73.78 (1) - 74.68 (1)	**85.06 (4)** - **85.04 (4)**	74.54 (1) - 74.53 (1)	76.36 (6) - 78.54 (6)	83.0 (4) - 84.89 (6)
r. door	57.72 (1) - 65.94 (4)	53.58 (4) - 58.63 (3)	**63.83 (4)** - **69.3 (4)**	50.1 (6) - 45.14 (1)	53.29 (6) - 41.27 (4)	50.71 (6) - 43.13 (6)
sidewalk	76.46 (6) - 74.99 (6)	79.76 (1) - 79.85 (1)	87.86 (4) - 87.42 (4)	79.11 (1) - 80.05 (1)	87.56 (4) - 87.14 (4)	**88.28 (6)** - **88.03 (6)**
street	77.28 (1) - 74.91 (1)	85.85 (1) - 85.9 (1)	90.72 (4) - **90.78 (4)**	71.02 (1) - 68.67 (1)	**90.88 (4)** - 90.55 (4)	90.81 (6) - 90.5 (6)
grass	84.12 (6) - 82.76 (6)	79.75 (1) - 77.38 (1)	88.79 (4) - 87.97 (4)	91.1 (1) - 89.1 (1)	95.59 (4) - 93.6 (4)	**96.36 (6)** - **94.91 (6)**
tree	31.74 (6) - 32.55 (6)	38.47 (4) - 38.37 (4)	**40.92 (1)** - 40.21 (6)	25.34 (1) - 28.09 (1)	33.7 (1) - 35.08 (1)	39.45 (1) - **41.34 (1)**
	PRECISION					
	Area 1 - *Area 1* hidden			*Area 2* - *Area 2* hidden		
	oblique	nadir	combined	oblique	nadir	combined
facade	**75.23 (1)** - **75.84 (1)**	61.32 (1) - 62.59 (1)	66.9 (1) - 68.04 (1)	73.77 (1) - 74.81 (1)	66.71 (6) - 64.7 (6)	68.33 (1) - 69.01 (1)
window	**64.97 (1)** - **65.13 (1)**	54.16 (1) - 56.04 (1)	60.75 (1) - 62.14 (1)	63.77 (1) - 63.84 (1)	56.53 (6) - 55.17 (6)	59.09 (1) - 59.16 (1)
door	**59.1 (1)** - **58.75 (1)**	42.31 (4) - 43.6 (4)	47.34 (1) - 46.05 (1)	55.49 (1) - 54.64 (1)	49.25 (6) - 45.61 (6)	48.06 (4) - 48.44 (6)
roof	81.56 (1) - 80.58 (1)	77.05 (1) - 74.96 (1)	**84.08 (4)** - 80.21 (4)	83.21 (1) - **83.35 (1)**	78.56 (1) - 77.46 (1)	81.16 (6) - 80.91 (6)
r. window	78.96 (1) - 80.13 (1)	70.18 (1) - 72.01 (1)	79.43 (4) - 78.29 (4)	**81.25 (1)** - 83.9 (1)	80.25 (1) - 82.71 (1)	80.65 (1) - **84.08 (1)**
r. door	63.5 (1) - 62.5 (1)	48.32 (1) - 55.11 (4)	54.66 (1) - 59.58 (1)	**65.19 (1)** - **63.67 (1)**	45.04 (6) - 40.6 (4)	45.99 (6) - 40.99 (1)
sidewalk	**88.51 (1)** - **88.48 (1)**	80.37 (1) - 81.26 (1)	83.35 (4) - 83.16 (1)	87.79 (1) - 87.55 (1)	83.66 (4) - 83.26 (4)	82.67 (6) - 82.32 (6)
street	**90.97 (1)** - **90.86 (1)**	83.27 (1) - 83.28 (1)	86.43 (4) - 86.35 (4)	87.23 (1) - 86.92 (1)	86.71 (4) - 86.46 (4)	85.91 (6) - 85.87 (6)
grass	92.32 (1) - 91.33 (1)	84.18 (1) - 82.37 (1)	89.35 (4) - 88.73 (4)	95.91 (1) - **94.75 (1)**	**96.11 (4)** - 94.39 (4)	95.88 (4) - 94.15 (6)
tree	78.37 (1) - 77.2 (1)	75.41 (4) - 75.15 (4)	74.22 (1) - 72.94 (1)	**80.73 (1)** - **80.49 (1)**	77.41 (6) - 76.66 (6)	77.63 (1) - 77.23 (1)
	RECALL					
	Area 1 - *Area 1* hidden			*Area 2* - *Area 2* hidden		
	oblique	nadir	combined	oblique	nadir	combined
facade	47.64 (1) - 45.78 (1)	63.92 (4) - 62.69 (4)	72.38 (4) - 71.14 (4)	60.48 (6) - 56.97 (6)	68.72 (6) - 66.99 (6)	**77.28 (6)** - **75.63 (6)**
window	53.75 (1) - 52.58 (1)	62.35 (4) - 61.28 (4)	**78.64 (4)** - 77.22 (4)	56.4 (6) - 54.72 (6)	67.99 (6) - 67.96 (6)	77.05 (6) - **77.71 (6)**
door	40.86 (6) - 40.72 (6)	65.95 (4) - 66.12 (4)	68.76 (4) - 67.99 (4)	51.1 (6) - 54.05 (6)	59.37 (6) - 58.03 (6)	**68.94 (6)** - **68.34 (6)**
roof	80.03 (1) - 76.27 (6)	83.82 (4) - 83.92 (4)	**92.25 (4)** - **91.65 (4)**	80.08 (6) - 81.01 (6)	87.8 (6) - 88.35 (6)	91.57 (6) - 90.72 (6)
r. window	75.76 (1) - 84.01 (6)	77.75 (1) - 77.57 (1)	**91.54 (4)** - 93.07 (4)	70.23 (6) - 72.07 (6)	79.95 (6) - 84.97 (6)	85.78 (4) - **87.82 (6)**
r. door	56.41 (4) - 71.34 (4)	63.3 (3) - 70.56 (3)	**83.51 (4)** - **92.79 (4)**	60.73 (6) - 35.79 (6)	65.25 (6) - 42.42 (6)	65.8 (4) - 56.62 (6)
sidewalk	79.36 (6) - 77.95 (6)	90.37 (4) - 91.4 (4)	92.88 (4) - 92.56 (4)	84.66 (6) - 84.74 (6)	93.77 (6) - 93.31 (6)	**94.71 (6)** - **94.59 (6)**
street	80.46 (6) - 79.17 (6)	92.97 (4) - 92.75 (4)	95.45 (4) - **95.68 (4)**	77.66 (6) - 73.99 (6)	95.47 (4) - 95.05 (4)	**96.31 (6)** - 95.66 (6)
grass	81.14 (6) - 79.23 (6)	75.77 (1) - 74.63 (4)	88.45 (6) - 87.43 (6)	86.75 (1) - 84.09 (1)	95.08 (4) - 92.82 (4)	**96.88 (6)** - **95.67 (6)**
tree	20.94 (6) - 21.65 (6)	25.82 (4) - 25.8 (6)	**29.44 (2)** - 28.76 (2)	15.03 (1) - 17.01 (1)	21.62 (1) - 22.82 (1)	26.58 (2) - **30.28 (2)**

Table 3: **Quantitative results per urban element.** Results for F score (top), precision (middle) and recall (bottom) for *Area 1* and *Area 2* at d=25cm. Each row gives the result for a particular class, first in the whole area and then in the hidden area, separated with a hyphen. The best score obtained among the pipelines is shown with the pipeline that generated it in brackets, numbered as in Fig. 4. In bold, the best measurement per class among all the image sets in both areas. Pipelines are as follow: (1) COLMAP + COLMAP, (2) COLMAP + OpenMVS, (3) OpenMVG-g + COLMAP, (4) OpenMVG-g + OpenMVS, (5) OpenMVG-i + COLMAP, (6) OpenMVG-i + OpenMVS.

bined imagery, OpenMVG-g + OpenMVS and OpenMVG-i + OpenMVS have the highest F score: the former in *Area 1* and latter in *Area 2*. Fig. 6 also includes the qualitative results of the point clouds obtained for the combined dataset in *Area 1* rendered under the same configuration (e.g., point size, shading) to make them comparable. From these results, we can observe that the point cloud obtained with COLMAP + COLMAP (Fig. 6 (a)) is sharper than the one obtained with COLMAP + OpenMVS (Fig. 6 (b)), in accordance with the precision values (74.89 and 27.93, respectively). Moreover, there are also differences in the completeness of the reconstructions: OpenMVG-i + OpenMVS (Fig. 6 (f)) and OpenMVG-g + OpenMVS (Fig. 6 (d)) are denser than the rest, and they also seem to be accurate. As before, the F score values confirm these observations, where they obtained the highest scores (79.36 and 76.76).

Urban category centric evaluation. Additionally, in Table 3 we present a summary of the same measurements calculated above (precision, recall and F score) but this time per urban element category. This summary shows three tables, one per measurement, where each row has the results of a specific class (i.e., urban category) and each column corresponds to a unique set of images. The result presented per cell in the table is the maximum score obtained among the six pipelines tested (see Fig. 4) and the pipeline that generate it is shown in brackets. The results for the complete area and the hidden one are presented in the same cell, in that order, separated by a hyphen.

Analyzing the results that were obtained per class across all the image sets available, we can observe that the method that most frequently gets the maximum precision is COLMAP + COLMAP. Those results are different when looking at recall. In that case, the pipeline OpenMVG-i + OpenMVS is the one that more frequently achieves the highest scores. When looking at the F score, we cannot identify a clear predominant pipeline for each class. In all the scenarios, the class with lowest F score values is tree and the results are really influenced by the low values of the recall. These results confirm the hypothesis in (Zolanvari et al., 2019): trees in the parks of the city can degrade the scores of the reconstructions. We can also analyze the results related to the image set under study. For example, with the combined set, the pipeline with best performance in the majority of classes is OpenMVG-g + OpenMVS in *Area 1* and OpenMVG-i + OpenMVS in *Area 2*. These results are in accordance with the ones commented before, which does not consider the class information (Table 2).

There is a different case scenario when we look at the results with the nadir images. In *Area 2* the scores from the OpenMVG-i + OpenMVS pipeline are the highest in most of the classes but it is not the best pipeline in the scene level evaluation. This is because OpenMVG-i + OpenMVS is the best with the facade class, with 11.10% of occupancy in the ground-truth (see Table 1), but also in classes with 1.23% of occupancy or less. However, OpenMVG-g + OpenMVS achieves the highest scores in the classes grass, sidewalk and street (16.24%, 11.18% and 10.57% of occupancy, respectively) and they also have the highest scores among all the classes. Also, if we look at the scores per class with the combined set in *Area 1*, COLMAP + COLMAP and OpenMVG-g + OpenMVS obtain the highest F scores in the same number of classes. This time, the most populated classes are the ones where COLMAP + COLMAP is better. These results reflect the importance of incorporating an object-category centric evaluation since a more detailed analysis can be done. The results of the evaluation per urban category in the hidden part (also depicted in Table 3) are different from the ones with the whole area but still follow the same pattern. For example, we can observe that the method that generates the best results per image set and class remains constant for the majority of them except for the door class. This is due to its small amount of samples.

Evaluation of pipeline components. We can also observe that, in general, the pipelines that obtained the best results are COLMAP + COLMAP, OpenMVG-g + OpenMVS and OpenMVG-i + OpenMVS. These results are in accordance with previous studies that used the same kind of metric, where COLMAP + COLMAP and OpenMVG-i + OpenMVS obtained the best results (Knapitsch et al., 2017). In particular, in that study OpenMVG-g + OpenMVS never has better results than COLMAP + COLMAP, but this situation is plausible in our study given the different camera trajectories (aerial grid configuration vs circle around an object), software versions and parameters used. COLMAP used as MVS is better than OpenMVS only if it is applied after COLMAP SfM. Whereas OpenMVS is better using the other SfM methods tested. This leads to the necessity to test not only a particular MVS method but a complete pipeline since it is going to be influenced by: the results obtained in the SfM step, the data conversion and preparation for the MVS step, as well as memory and computing limitations. In this benchmark, the results after each step are not evaluated because, as explained in Section 4, we want to enforce the creation of end-to-end solutions and we do not focus on any particular part of a pipeline. Sim-

ilarly, specific processing times are not reported but for all the pipelines it was in the order of hours due to the quantity of images that had to be processed.

6 CONCLUSION

In this paper, we have presented a novel benchmark for evaluating image-based 3D reconstruction pipelines with aerial images in urban environments. The results obtained with the considered SfM+MVS state-of-the-art pipelines are evaluated at scene level and per urban category. This allows for further analysis of the reconstructions (i.e., analysis of the influence of each urban category in the scene level scores) and it supports previous hypothesis (e.g., parks can degrade the F score values in a scene level evaluation) with quantitative measurements. Also, we provide the means for evaluating results in a hidden area to avoid fine tuning of algorithms to the given ground truth. Furthermore, we stimulate and support the evaluation of new approaches for image-based 3D reconstruction as we do not limit the evaluation to a specific stage of the pipeline (e.g., MVS). Finally, to support the progress of research in the community we provide the dataset and an online evaluation platform at https://v-sense.scss.tcd.ie/research/6dof/benchmark-3D-reconstruction.

ACKNOWLEDGEMENTS

This publication has emanated from research conducted with the financial support of Science Foundation Ireland (SFI) under the Grant Number 15/RP/2776.

REFERENCES

Aanæs, H., Jensen, R. R., Vogiatzis, G., Tola, E., and Dahl, A. B. (2016). Large-scale data for multiple-view stereopsis. *International Journal of Computer Vision*.

Barnes, C., Shechtman, E., Finkelstein, A., and Goldman, D. B. (2009). Patchmatch: A randomized correspondence algorithm for structural image editing. In *ACM Transactions on Graphics (ToG)*. ACM.

Bosch, M., Foster, K., Christie, G., Wang, S., Hager, G. D., and Brown, M. (2019). Semantic stereo for incidental satellite images. In *WACV 2019*. IEEE.

Furukawa, Y. and Ponce, J. (2010). Accurate, dense, and robust multiview stereopsis. *IEEE Transactions on Pattern Analysis and Machine Intelligence*.

Hartley, R. and Zisserman, A. (2003). *Multiple view geometry in computer vision*. Cambridge University Press.

Jancosek, M. and Pajdla, T. (2011). Multi-view reconstruction preserving weakly-supported surfaces. In *CVPR 2011*. IEEE.

Knapitsch, A., Park, J., Zhou, Q.-Y., and Koltun, V. (2017). Tanks and temples: Benchmarking large-scale scene reconstruction. *ACM Transactions on Graphics*.

Laefer, D. F., Abuwarda, S., Vo, A.-V., Truong-Hong, L., and Gharibi, H. (2015). 2015 aerial laser and photogrammetry survey of dublin city collection record.

Menze, M. and Geiger, A. (2015). Object scene flow for autonomous vehicles. In *CVPR 2015*.

Moulon, P., Monasse, P., and Marlet, R. (2012). Adaptive structure from motion with a contrario model estimation. In *ACCV 2012*. Springer Berlin Heidelberg.

Moulon, P., Monasse, P., and Marlet, R. (2013). Global fusion of relative motions for robust, accurate and scalable structure from motion. In *ICCV 2013*.

Munoz, D., Bagnell, J. A., Vandapel, N., and Hebert, M. (2009). Contextual classification with functional max-margin markov networks. In *CVPR 2009*.

Özdemir, E., Toschi, I., and Remondino, F. (2019). A multi-purpose benchmark for photogrammetric urban 3d reconstruction in a controlled environment.

Pagés, R., Amplianitis, K., Monaghan, D., Ondřej, J., and Smolić, A. (2018). Affordable content creation for free-viewpoint video and vr/ar applications. *Journal of Visual Communication and Image Representation*.

Rottensteiner, F., Sohn, G., Gerke, M., Wegner, J. D., Breitkopf, U., and Jung, J. (2014). Results of the isprs benchmark on urban object detection and 3d building reconstruction. *ISPRS journal of photogrammetry and remote sensing*.

Ruano, S., Cuevas, C., Gallego, G., and García, N. (2017). Augmented reality tool for the situational awareness improvement of uav operators. *Sensors*.

Ruano, S., Gallego, G., Cuevas, C., and García, N. (2014). Aerial video georegistration using terrain models from dense and coherent stereo matching. In *Geospatial InfoFusion and Video Analytics IV; and Motion Imagery for ISR and Situational Awareness II*. International Society for Optics and Photonics.

Schönberger, J. L. and Frahm, J.-M. (2016). Structure-from-motion revisited. In *CVPR 2016*.

Schönberger, J. L., Zheng, E., Pollefeys, M., and Frahm, J.-M. (2016). Pixelwise view selection for unstructured multi-view stereo. In *ECCV 2016*. Springer.

Schops, T., Schonberger, J. L., Galliani, S., Sattler, T., Schindler, K., Pollefeys, M., and Geiger, A. (2017). A multi-view stereo benchmark with high-resolution images and multi-camera videos. In *CVPR 2017*.

Seitz, S. M., Curless, B., Diebel, J., Scharstein, D., and Szeliski, R. (2006). A comparison and evaluation of multi-view stereo reconstruction algorithms. In *CVPR 2006*.

Serna, A., Marcotegui, B., Goulette, F., and Deschaud, J.-E. (2014). Paris-rue-madame database: a 3d mobile laser scanner dataset for benchmarking urban detection, segmentation and classification methods.

Snavely, N., Seitz, S. M., and Szeliski, R. (2008). Modeling the world from internet photo collections. *International Journal of Computer Vision*.

Stathopoulou, E. K., Welponer, M., and Remondino, F. (2019). Open-source image-based 3d reconstruction pipelines: review, comparison and evaluation. *The International Archives of Photogrammetry, Remote Sensing and Spatial Information Sciences*.

Strecha, C., Von Hansen, W., Van Gool, L., Fua, P., and Thoennessen, U. (2008). On benchmarking camera calibration and multi-view stereo for high resolution imagery. In *CVPR 2008*.

Sweeney, C., Hollerer, T., and Turk, M. (2015). Theia: A fast and scalable structure-from-motion library. In *Proceedings of the ACM International Conference on Multimedia*, pages 693–696. ACM.

Vallet, B., Brédif, M., Serna, A., Marcotegui, B., and Paparoditis, N. (2015). Terramobilita/iqmulus urban point cloud analysis benchmark. *Computers & Graphics*.

Zhang, L., Li, Z., Li, A., and Liu, F. (2018). Large-scale urban point cloud labeling and reconstruction. *ISPRS Journal of Photogrammetry and Remote Sensing*.

Zolanvari, S., Ruano, S., Rana, A., Cummins, A., da Silva, R. E., Rahbar, M., and Smolic, A. (2019). Dublincity: Annotated lidar point cloud and its applications. *30th BMVC*.